GeoScienceWorld
Lithosphere
Volume 2022, Article ID 9049312, 19 pages
https://doi.org/10.2113/2022/9049312

Lithosphere

Research Article

Evaluation of Natural Gas Hydrate Fault System: A Case from a Sag in Deep-Water Slope Area of the Northern South China Sea

Shuang Mao,[1,2] **Guangming Hu**,[1] **Liguo Hu**,[3] **Pengqi Liu**,[4,5] **Xu Chen**,[1] **and Min Qin**[6]

[1]*School of Geosciences, Yangtze University, Wuhan 430100, China*
[2]*Economics & Technology Research Institute of Liaohe Oilfield Company, PetroChina, Panjin 124000, China*
[3]*Exploration Division of Liaohe Oilfield Company, PetroChina, Panjin 124000, China*
[4]*Sanya Institute of South China Sea Geology, Guangzhou Marine Geological Survey, Sanya 572025, China*
[5]*Academy of South China Sea Geological Science, China Geological Survey, Sanya 572025, China*
[6]*Exploration & Development Research Institute of Liaohe Oilfield Company, PetroChina, Panjin 124000, China*

Correspondence should be addressed to Guangming Hu; hugm@yangtzeu.edu.cn

Received 11 May 2022; Revised 19 October 2022; Accepted 1 November 2022; Published 6 December 2022

Academic Editor: Feng Cheng

The fault system is one of the structural carrier systems of gas hydrate accumulation, which plays a vital role in controlling the distribution of natural gas hydrate (NGH) accumulation. The previous studies mainly focus on summarizing the vertical migration mode of high flux fluid along the fault with obvious geophysical response characteristics on the seismic profile, such as "fault with gas chimney," "fault with mud diapir," and "fault with submarine collapse", but lack of evaluation methods for the fault carrier system. We use the X sag in the deep-water continental margin slope area of the northern South China Sea as an example to study the fault systems closely related to NGH. This paper puts to use attribute technologies, such as coherence, curvature, and fusion, to analyze the characteristics and combination of the fault systems. We discussed migration patterns and evaluation methods of dominant fault carrier systems. This research proves that the strike-slip fault system in the platform area can directly connect the gas source bed with high-quality hydrocarbon generation to the gas hydrate stability zone (GHSZ). The activity of this fault system is more conducive to the accumulation of hydrocarbon in the GHSZ. This area has a good site for pore-filling gas hydrate prospecting and a preferential favorable fault carrier system. The composite fault system, consisting of a normal dip-slip fault system and a polygonal fault system, in the slope area can jointly communicate the biogenic gas-rich reservoir. Its activity and well-migration performance are the main reasons for the submarine gas leakage and collapse. It is a secondary favorable fault carrier system in the study area. There may be massive and vein natural gas hydrate formation in fractures in the leakage passage, and pore-filled gas hydrate may exist in the submarine nonleakage area. In this work, a three-factor evaluation method of the fault carrier system is proposed for the first time. This method is of great significance for the evaluation and exploration of NGH reservoirs in the continental margin slope area of the northern South China Sea.

1. Introduction

Natural gas hydrates (NGH) are solid minerals formed by low molecular weight gases such as methane and water molecules under high-pressure and low-temperature environments. It mainly developed inland permafrost and marine sediments with a water depth of more than 300 m [1, 2]. The research on NGH is of great significance to the economy and environmental protection. China began to systematically investigate and research gas hydrate in the South China Sea in the late 1990s. Qiongdongnan Basin and its adjacent areas have always been the key areas. Guangzhou Marine Geological Survey (GMGS) has carried out much research on geological, geophysical, and geochemical in the basin [3–5]. Two rounds of trial production were successfully conducted [6–9], which confirmed the considerable exploration

potential of NGH in the continental margin slope area of the northern South China Sea [10–14].

Fault, diapir structure, gas chimney, and high permeability layer are generally considered as the main channels for hydrocarbon fluid migration, while the fault is generally considered as the most fundamental channel for accumulation fluid migration [15, 16]. NGH exploration research found that faults, as channels with high permeability, play a crucial role in the upward migration of deep hydrocarbon fluids to form hydrate reservoirs, and to a large extent, determine the distribution of hydrate [17–27]. The previous studies mainly focus on summarizing the vertical migration mode of high flux fluid along the fault with obvious geophysical response characteristics on the seismic profile, such as "fault with gas chimney," "fault with mud diapir," "fault with submarine collapse," and lack of research on hydrate transport conductor system with only fault development and evaluation methods for fault carrier system. In this paper, we use the X sag in the deep-water continental margin slope area of the northern South China Sea as an example to study the fault systems closely related to NGH. Attribute technologies, such as coherence, curvature, and fusion, were put to use for analyzing characteristics, classifications, and combinations of the fault system. We discussed migration patterns and evaluation methods of fault carrier systems. Finally, favorable exploration zones are predicted.

2. Geologic Setting

The study area is located at the continental margin slope area in the deep-water of the northern South China Sea (Figure 1). The area is affected by the interaction of the Pacific plate, the India-Australia plate, the Eurasian plate, and the expansion of the South China Sea [28–34]. Previous studies have shown that three tectonic events controlled the formation and evolution of the area since the Cenozoic (Figure 2): the continental margin cracking at the end of the Mesozoic, the South China Sea expansion in the late Oligocene, and the plate wedging event at the end of mid-Miocene [35–37]. At the end of the Mesozoic, the Pacific plate was subducted from the east to the Eurasian plate and then retreated. The upper mantle material arched up, resulting in the cracking of the continental margin, forming a NE-SW Cenozoic-faulted basin in the north of the South China Sea. Since then, the northern basin of the South China Sea has entered the rifting stage (T_g-T_{51}). From east to west, Taixinan Basin, Pearl River Mouth Basin, Beibuwan Basin, Qiongdongnan Basin, and Yinggehai Basin are developed [38–41]. During the rifting stage, the fault arrays are trended in NE, controlling the strike of main structural units and the deposition of the strata in this area. The sedimentary sag shows strong separation, and two dustpan-like depressions and a low uplift structural unit are developed. In the late Oligocene, the India-Australia plate collided with the Eurasian plate, and the mantle flows slowly dispersed and accumulated to the southeast [42–44], resulting in large-scale extensional activities on the continental margin of South China. The continental crust gradually thinned and ruptured, forming the South China Sea oceanic crust, and the South China Sea ocean basin began to expand in the north-south direction [36, 37]; then, an NW-trending strike-slip fault array occurred in this area. After this event, the crust in the west of the South China Sea continued to thin under the action of strike-slip action and tension. However, the tectonic activity weakened, the faults were less developed, and the area entered the transition stage (T_{51}-T_3). In transition stage, the influence of deep faults on the tectonic units and sedimentation gradually weakened. At the end of the mid-Miocene, the force of the Pacific plate on the Eurasian plate gradually strengthened, and the India-Australia plate continued to wedge northward [45]. Then, the South China block squeezed eastward, and the Indosinian block rotated clockwise, resulting in the Dongsha movement [45, 46]. The Dongsha movement is in the north of the South China Sea, and the Wan'an movement is in the south of the South China Sea [32]; the NW-trending strike-slip faults were still active. After this event, the expansion of the South China Sea ocean stopped, the faults were undeveloped, and the area entered the regional subsidence stage (T_3-T_0). At the end of the late Miocene (near T_2), the Indosinian block wedged into the Eurasian plate and is in a relatively stable state. Meanwhile, the Indosinian block has strengthened its influence on the South China block, resulting in the overall eastward extrusion of the South China block. The activity of the Indosinian block changed the strike-slip activity of the Honghe-Yinggehai fault in the west of the South China Sea from left to right [47–49], resulting in the tectonic uplift in this area. Tectonic uplift is the reason for the formation of geomorphic units in regional strata, such as platform, slope, and trough. Tectonic uplift and strike-slip activities make the region form normal dip-slip faults and strike-slip faults.

The Yacheng group and the Lingshui group were filled in rifting period, which is a set of clastic rock mudstone deposits of shore facies shallow sea shelf facies. In the transition period, the Lingshui I and II group, the Sanya group, and the Meishan group were filled, which is a set of shallow sea bathyal facies mudstone intercalated with calcareous mudstone deposits. During the regional subsidence period, the Huangliu group, the Yinggehai group, and the Ledong group were filled, which is a set of mudstone deposits of bathyal facies [50, 51].

Four sets of gas source beds were developed in the study area (Figure 2). By calculation, the Yacheng group (T_6-T_{52}) has the highest organic matter abundance and high maturity. With generating biogas at about 25 Ma, it quickly entered into the peak of hydrocarbon generation from 15 Ma and generating biogas slowly now [52–54]. The cumulative hydrocarbon generation of this set of gas source beds is significant, but it is far away from the gas hydrate stability zone (GHSZ). With few communication faults, we considered that it has little contribution to the gas source of NGH accumulation. The organic matter abundance of the Lingshui III group (T_{52}-T_{51}) is good. It started to generate biogas at about 15 Ma, entered the peak hydrocarbon generation at about 8 Ma, and stopped generating biogas at about 5 Ma. It has enormous hydrocarbon generation and is the primary gas source bed [55, 56]. The vertical layer from the Lingshui I and II group to the Meishan group

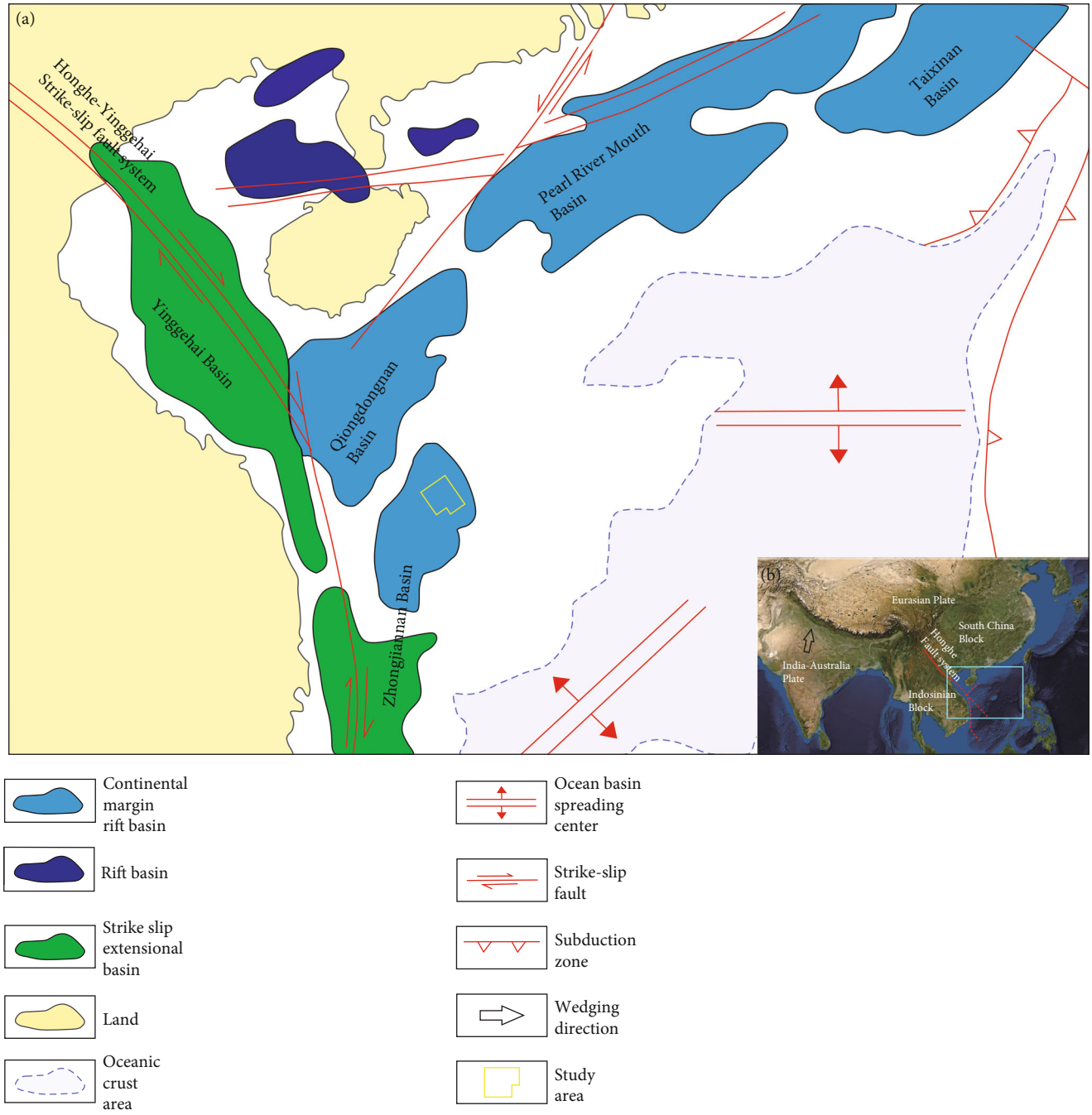

FIGURE 1: Location of the study area and distribution of Honghe-Yinggehai strike-slip fault. (a) The figure describes the characteristics of basin types and distribution in the northern slope area of the South China Sea, the distribution of the Honghe-Yinggehai strike-slip fault, and the oceanic crust and its expansion center [30, 33]. (b) The base map is from Google Earth, and the red line in the figure shows the Honghe strike-slip fault, and the red-dotted line shows the extension of the Honghe strike-slip fault in the South China Sea [36, 37]).

(T_{51}-T_3) has a good abundance of organic matter. Biogas generation started at about 10 Ma and peaked at about 5 Ma. After that, the hydrocarbon generation intensity decreased. However, it continues to generate biogas now. It has an enormous hydrocarbon generation intensity and is the primary gas source bed. The organic matter abundance of the Huangliu group (T_3-T_2) is poor. It began to generate biogas at about 10 Ma and entered the peak hydrocarbon generation at about 4 Ma. However, the hydrocarbon generation intensity of this set of gas source beds is low, which may have little contribution to the gas source of NGH accumulation.

3. Data and Method

Data used in this study consist of the following: (1) about 1560km^2 of full offset, poststack time migrated (PSTM) seismic data, and has a total trace length of 7 s TWT. Processing

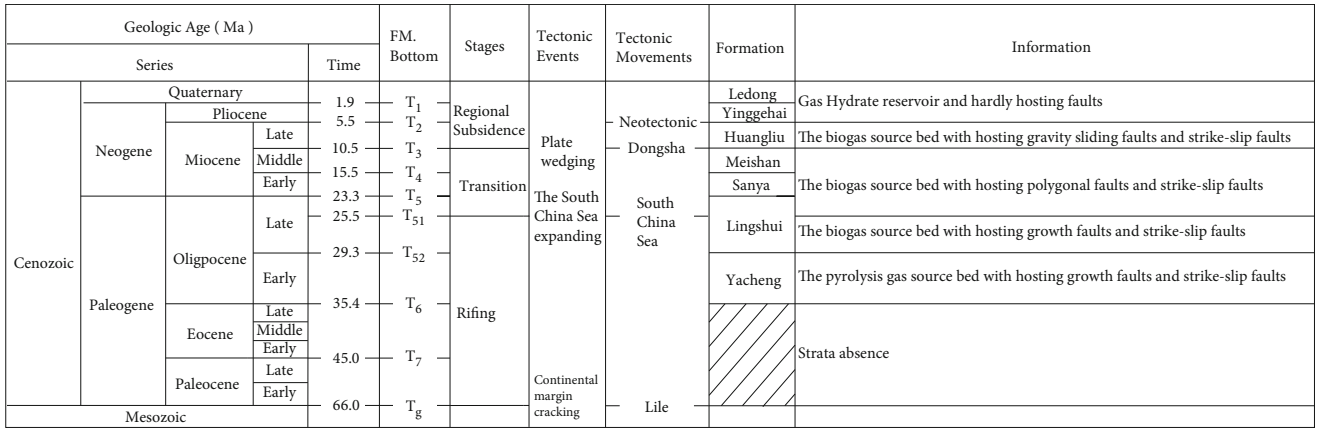

Figure 2: Division of regional tectonic events and evolution stages in the study area. Note: 8.2 Ma indicates the boundary time between the upper and lower members of the Huangliu group; 3 Ma indicates the boundary time between the upper and lower parts of the Yinggehai group. Age from article [28, 48, 57]; tectonic events form article [19, 20, 35–37, 58].

steps included signal noise reduction and corrections and velocity analysis using Kirchhoff PSTM; (2) time-depth charts complied from the wells previously drilled in the basin to calculate fault characteristic data like fault offset, dip angle, and extension length; (3) seabed temperature, formation pressure, and geothermal gradient data were used for modeling the thickness of the GHSZ in the study area.

Seismic interpretation and attributes were chosen to visualize as follows: (1) signs of fault activity, such as (a) traction deformation in attribute fusion and (b) geomorphological marks of the submarine failures on the seafloor; (2) sedimentary sequence; (3) seismic indicators of gas hydrate and associated gas/fluids, such as (a) BSR, (b) buried collapses that do not reach the seafloor, and (c) gas seep forming collapses on the seafloor.

The process of this research is as follows:

(i) *Extracting the dip and azimuth, coherent, and curvature attributes*. Dip angle and azimuth volume are the basis for extracting attribute volumes of curvature, coherence, and structure-oriented filtering. In 3D seismic data interpretation, an accurate time-depth conversion relationship is usually not available. Through the multiwindow scanning technology, the window with the largest similarity can be obtained as the dip and azimuth estimation window of the analysis point, which can improve the calculation accuracy and the stability of the calculation results. Directional filtering is carried out along layers by using dip and azimuth volumes to improve the signal-to-noise ratio of seismic data, make the continuity and discontinuity of seismic data more obvious, and improve the reliability of horizon tracking. Coherence is one of the most useful attributes for seismic fault and fracture detection at present. Its technical principle is to calculate the data coherence in the time window for each time window in the migrated 3D seismic data and assign this result to the central sample point of the time window and finally form 3D data representing the coherence. The similarity of the local seismic waveform is compared through 3D data, and the points with low coherence values are related to the discontinuity of the reflected wave shape. Based on the high signal-to-noise ratio of seismic data and the characteristics of target layers, this work selected the 9-point algorithm of eigenvalue is selected to calculate the coherence cube. This method can obtain more important characteristic parameters such as faults and fractures and then improve the lateral resolution of faults. The curvature attribute can reflect the bending degree of the stratum. The greater the curvature value is, the higher the bending degree. The curvature is in direct proportion to the degree of fracture development to a certain extent. In this study, curvature attribute volume is mainly used to calculate the fault rose map and observe the degree of seabed deformation.

(ii) *Attribute fusion*. In this study, seismic data and coherence attribute are fused through a certain proportion to obtain a new attribute fusion data. The data contains the characteristic information of the coherence attribute and seismic information. Because the fusion data contains fault and strata characteristic information, it can reduce the uncertainty caused by using one data in interpretation. This method can obtain rich stratigraphic information and outstanding geological meaning, provide a basis for artificial identification of faults, and improve the interpretation reliability.

(iii) *Construct steering filter*. Directional filtering is carried out along layers by using dip and azimuth bodies to improve the signal-to-noise ratio of seismic data. It makes the continuity and discontinuity of seismic event more obvious and improves the reliability of horizon tracking.

(iv) *Fault interpretation and property analysis*. We interpreted faults by the fusion attribute and completed

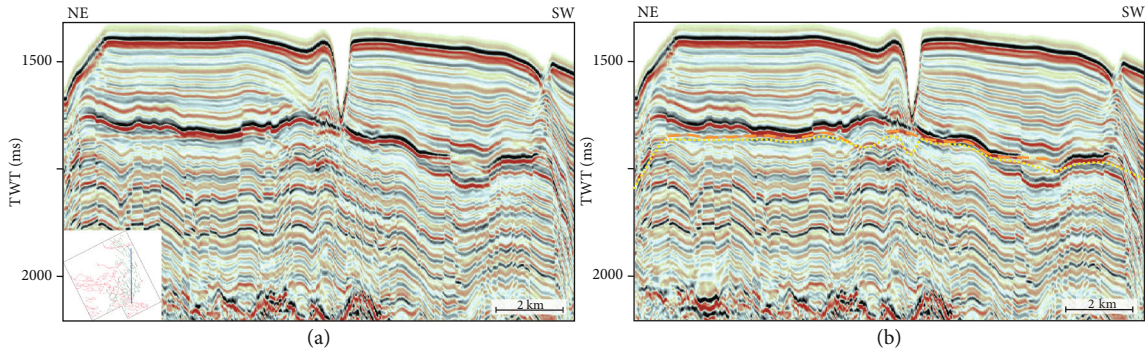

FIGURE 3: The characteristic of BSR and GHSZ. (a) The seismic profile. (b) The interpretation of BSR and GHSZ. The orange lines indicate BSR. and the yellow line indicates the bottom of GHSZ.

the fault combination on the plane. Through the analysis of regional stress, sedimentary and tectonic stages of the area, the characteristics of fault activity, element parameters, and distribution rules are determined. We discussed the origin and timing of the fault, providing a basis for the evaluation of the fault system.

4. Result

4.1. Bottom Simulating Reflector (BSR) and Gas Hydrate Stability Zone (GHSZ). BSR is one of the most critical geophysical identification marks of marine NGH, which refers to the reflection interface approximately parallel to the seabed on the seismic profile (Figure 3). The reflection interface is caused by the wave impedance difference between the hydrate-bearing sediments and the underlying sediments. BSR is basically parallel to the seabed, with opposite polarity and obvious layer crossing phenomenon. Most BSRs are approximately parallel to the strata or oblique at a small angle, with stable horizontal distribution and well continuity.

The zone where NGH is stable at temperature and pressure conditions beneath the sea floor can be termed as the GHSZ (Figure 3). The bottom depths of the GHSZ were previously calculated by five hydrate-drilled stations in the Shenhu area. The geothermal gradient was measured in situ at 45-67.7°C/km [59]. The suitable geothermal gradient creates favorable physical conditions for NGH accumulation. The BSR burial depth of four stations is in good agreement with the bottom boundary of the methane hydrate stability zone calculated by the equations of Miles (1995) [60, 61]. We infer the Miles methane hydrate phase curve equation is suitable for the calculation of methane hydrate stability region in the northern South China Sea. In this study, the GHSZ was calculated by the equations of Miles for hydraulic pressure property equilibrium using the following: (1) water depth data 900-1300 m, (2) data of bottom water temperatures 3-5.0°C and formation pressure measured over the area, and (3) constant geographical gradient values taken from a nearby site [62–65]. Through calculation, the geothermal gradient in the study area is about 53°C/km, which has stable conditions for NGH accumulation and enrichment. The bottom of the GHSZ is 140 m to 220 m below the seabed.

4.2. The Characteristics and Genesis of the Fault System. We completed the well-seismic calibration according to the drilling data in the adjacent area. We establish the stratigraphic sequence framework of the study area by analyzing seismic wave reflection characteristics of regional good sections. On this basis, the directional filtering and fine stratigraphic interpretation are carried out by extracting the dip and azimuth attributes, thus improving the signal-to-noise ratio of seismic data and the reliability of horizon tracking. Then, the fusion attribute data is put to use interpreting the faults. Finally, combined with the regional stress field and sedimentation and tectonic evolution in this area, this paper analyzes the fault characteristics of activity, element parameters, and distribution. We explain the genesis and timing to provide a basis for evaluating the fault system. We divided the fault arrays in the transition period and regional subsidence period into three fault systems: polygonal, gravity sliding, and strike-slip fault systems.

4.2.1. The Polygonal Fault System. The term polygonal refers to an extensional fault system developed in fine-grained sediments. It has the characteristics of layer-limited, nonstructural origin, slight fault offset, large dip angle, high density, variable plane strike, and intersecting in polygonal combination. It is also often called a layer-limited fault system [66–70]. The polygonal fault system in this area appears in the vertical layer, which formed during the transition period.

The fault array in the transition sedimentary strata has prominent layer-limited properties. Generally, in the process of the tectonic evolution of the basin, the tectonic stress in the transition stage is weaker than in the rift stage, and fault activities are less [71]. However, the fault density of the transition strata is much higher than that of the rift strata. The layer-limited fault has been formed in the whole area (Figure 4(a)). The seismic profile shows that most faults are limited to the transition strata (T_{51}-T_3), and their distribution is irrelevant to the structural units of rift strata. Most of them are not formed by the extension of faults in the rift stage (Figure 5). The vertical extension length of faults is controlled by the thickness of the transition strata. With

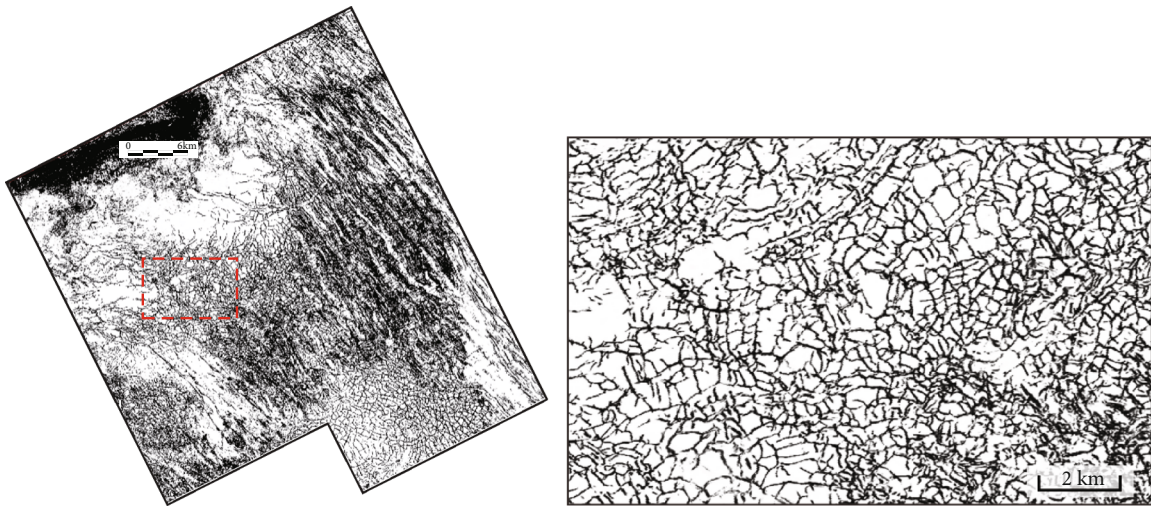

Figure 4: Distribution characteristics of polygonal fault system in the study area. (a) The plane distribution characteristics of the polygonal fault system are shown by the slice along the layer of coherence attribute volume T3, and the lower right corner is a typical polygonal fault. (b) The enlargement of the field of view of the dashed box in (a), which is also a typical polygon fracture.

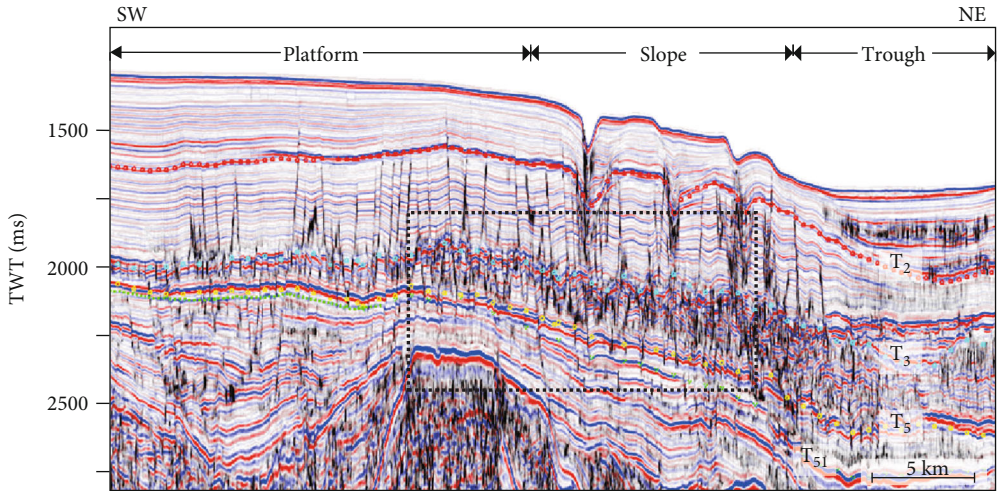

Figure 5: Attribute fusion data of conventional seismic data and coherent attribute data on AA's profile (location on Figure 6).

the strata in the northwest being thin, the vertical extension of the fault is short. With the strata in the southeast thick, the vertical extension of the fault is long (Figure 5). In addition, the density of the fault is large, the fault offset is slight (3 m to 15 m), the dip angle of the fault plane is high (50° to 90°), and the fault plane is flat. They are normal faults with a similar or opposite inclination. The top of the transition strata was cut by faults, showing wavy reflection characteristics in seismic profiles (Figures 5 and 6). On the plane, the fault strike is random, intersectant, and irregular (Figure 4(b)), in line with the general characteristics of polygonal faults [72].

The polygonal fault system originated from density inversion in the study area. A polygonal fault system in the Hope Lake region of South Australia originated from density inversion. It appeared in the mudstone sequence from the Cadna-owie formation to the Mackunda formation [72–74]. (a) The Cadna-owie formation developed a 35 m thickness and low-density mudstone. (b) The overlying mudstone of the Cadna-owie formation rapidly deposits, which hinders the dehydration and compaction of the low-density mudstone layer, and the low-density mudstone layer is gradually under compacted. (c) With the gradual strengthening of compaction, extensive overpressure occurs in the horizontal direction of the low-density mudstone layer. After exceeding the critical value, hydraulic cracks and faults were generated at the top of the overpressured layer. Then, overpressure was released gradually to form a polygonal system. (d) When the polygonal faults are forming, the pore water in the mudstone layer is mainly drained. Then, the pressure decreases, the volume of the mudstone layer gradually shrinks to the minimum, and the polygonal

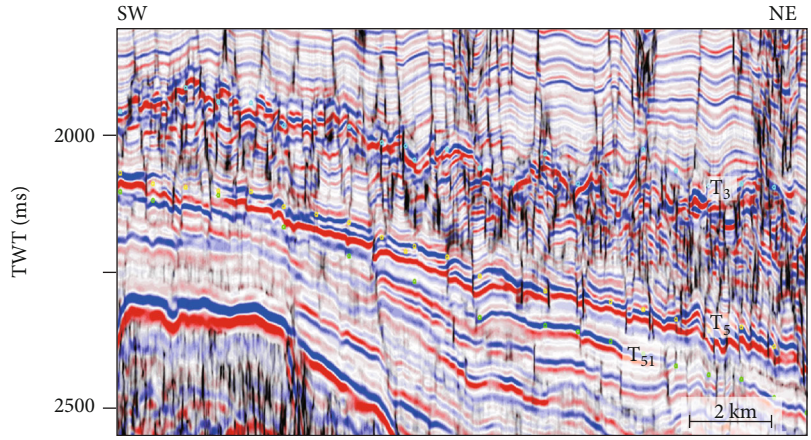

Figure 6: Enlarged profile of attribute fusion data (location on a dotted box of Figure 5).

faults closed and stop developing. As the deep fluid migrates upward, the pressure in the polygonal fault array accumulates again, and a new polygonal fault array is formed in the mudstone formation. Furthermore, the polygonal fault system is formed from the Cadna-owie formation to the Mackunda formation. (e) This process will cause the collapse at the top of the overpressure layer, which results in wavy seismic reflection at the top of the overpressure layer. The polygonal fault array geometry characteristics in the study area are similar to those in the Hope Lake area, South Australia; the top of the Lingshui I and II group is argillaceous limestone containing a thin layer of limestone, and the top of the Meishan group is developed with a thin layer of carbonate rock, resulting in a relatively low-density bathyal mudstone between the Lingshui I and II group to Meishan group; a polygonal fault array is developed from the Lingshui I and II group to the bottom of Meishan group, and the top of the fault array cuts the wavy seismic reflection. Therefore, we speculated that the polygonal fault system in the study area is of density inversion origin.

4.2.2. The Normal Dip-Slip Fault. The normal dip-slip fault refers to a fault system formed by the sliding of the rock stratum, which is controlled and influenced by gravity. The normal dip-slip fault system in this area appears in the regional subsidence strata at the slope area (Figures 7 and 8).

At the end of the late Miocene, the strike-slip activity of the Honghe-Yinggehai fault system in the western South China Sea [47–49] caused the tectonic uplift. It formed geomorphic units of platforms and slopes in this area. It leads to forming normal dip-slip faults in the slope area, which belongs to the tensile fault. The seismic profile shows that the fault array has the properties of positive dislocation. It breaks through the Huangliu group upward and reaches the Meishan group downward. Some can extend downward to the Sanya group. The fault array has the following characteristics such as low density (3 pieces/km to 5 pieces/km), large distance (5 m to 20 m), and high dip angle (34° to 70°). There is no apparent difference in the thickness of the two walls with the same fault. The fault system trends the NW-SE on the plane.

4.2.3. The Strike-Slip Fault System. The strike-slip fault system mainly appears in the platform area and is relatively less occurs in trough areas and slope areas (Figures 7 and 8).

Since the late Oligocene, the strike-slip faults have had properties of early tension and late compression. From the rift stage to the early regional subsidence stage, the strike-slip fault array is tensile in a nearly E-W trend (Figures 9(a) and 9(b)). The time slice profile of the attribute fusion data in the rift period shows that the strata on the north side of the fault have an NWW trend traction deformation (shown by the black arrow in Figure 10(a)). The stratum on the south side of the fault has a high degree of damage, indicating that the fault wall on the south side is relatively active. We speculate it is a sinistral left connecting fault with tensile and torsional properties. The strike-slip fault array is compressional in the NWW-SEE trend in the late regional subsidence strata. The profile of coherent attribute slices along a layer in the regional subsidence period shows that the derived faults are near the S-N trend (Figure 9(c)). The direction of the sharp-included angle indicates that the fault array is dextral. The associated secondary faults are on the northeast of principal strike-slip fault planes (Figure 11), illustrating that the fault wall on the northeast side is relatively active. We speculate that it is a left connecting dextral fault with compressive properties. The study area is on the offshore extension zone of the Honghe strike-slip fault system [47, 48]. We consider that the strike-slip fault system in this area has the same development and evolution characteristics as Honghe strike-slip fault system [47, 75]. The fault array shows positive dislocation on the seismic profile, which breaks through the Huangliu group upward and reaches the Lingshui III group downward, and some even go down through the basement (Figure 9). Most fault planes are gentle upward and steep downward. The main faults and associated secondary faults are combined into a negative flower shape or Y shape. The fault array in the regional subsidence period has the following

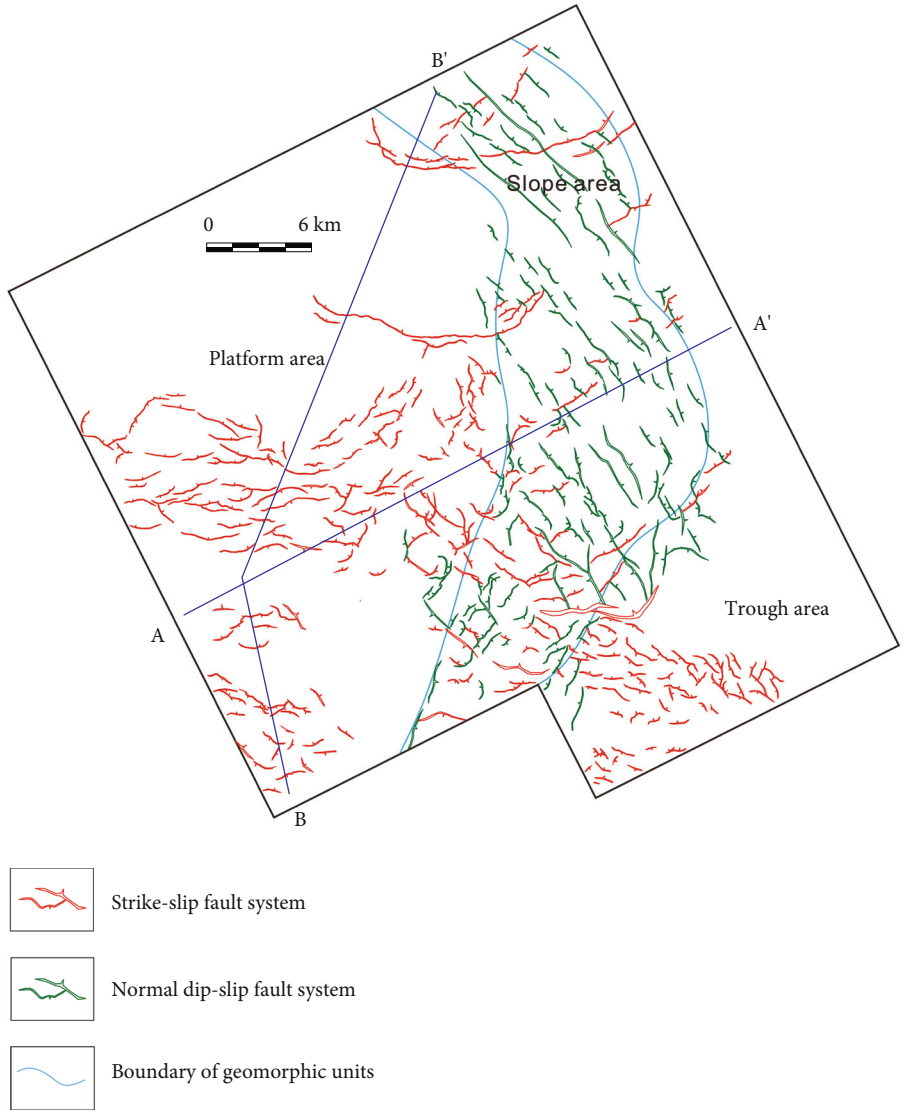

FIGURE 7: Distribution characteristics of normal dip-slip fault system and strike-slip fault system of a layer between T_3-T_2 in the study area; the trough area in the figure is in NW-SE trend, and most of it is distributed outside the study area.

characteristics such as low density (3 pieces/km to 5 pieces/km), small distance (12 m to 13 m), and low dip angle (38° to 57°).

The polygonal fault system is mainly affected by lithology, while the normal dip-slip fault system and the strike-slip fault system are mainly affected by regional strike-slip activities. Laterally, the polygonal fault system has the largest distribution area and the most significant fault density. The normal dip-slip fault system and the strike-slip fault system are distributed in different positions as belts, and their distribution area and fault density are the same (from a layer between T_3 and T_2). The polygonal fault system is vertically distributed in the middle strata with the smallest extension distance. The normal dip-slip fault system is distributed in the shallowest strata with a medium extension distance. The strike-slip fault system is distributed with the largest extension distance from bottom to top. The polygonal fault system has a minor fault offset in the space of fault activity, however, with a higher fault dip angle. The normal dip-slip fault system has the largest fault offset and high fault dip angle. The strike-slip fault system has a minor fault offset and a smaller dip angle.

5. Discussion

5.1. The Relationship between "Source to Zone" and Fault Carrier Systems. There are three types of fault systems in the study area. Different fault systems are located at different positions in the sequence framework and play different roles in the process of hydrocarbon migration.

The polygonal fault system connects the gas source bed of the Lingshui I and II group, the Sanya group, and the Meishan group (T_{51}-T_3), with a wide distribution (Figures 4 and 12). It can become a practical path for lateral and large-scale diffusive migration of hydrocarbons.

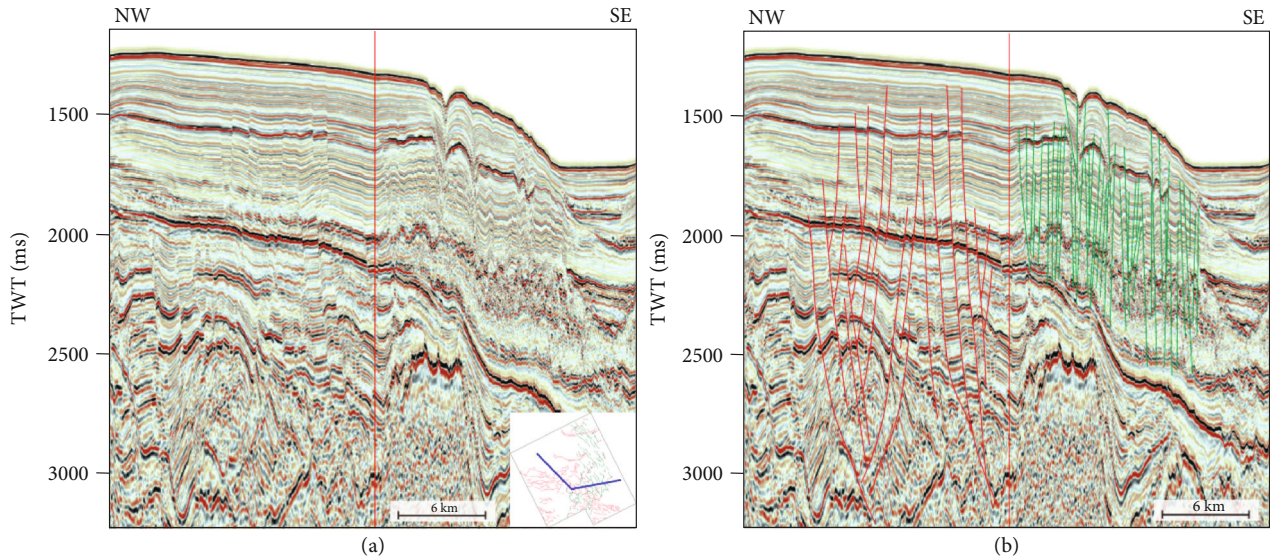

Figure 8: (a) The characteristics of normal dip-slip fault array and strike-slip fault array in seismic profile. (b) The interpretation of normal dip-slip fault and strike-slip fault. The red lines indicate a strike-slip fault array, and the green lines indicate a normal dip-slip fault array.

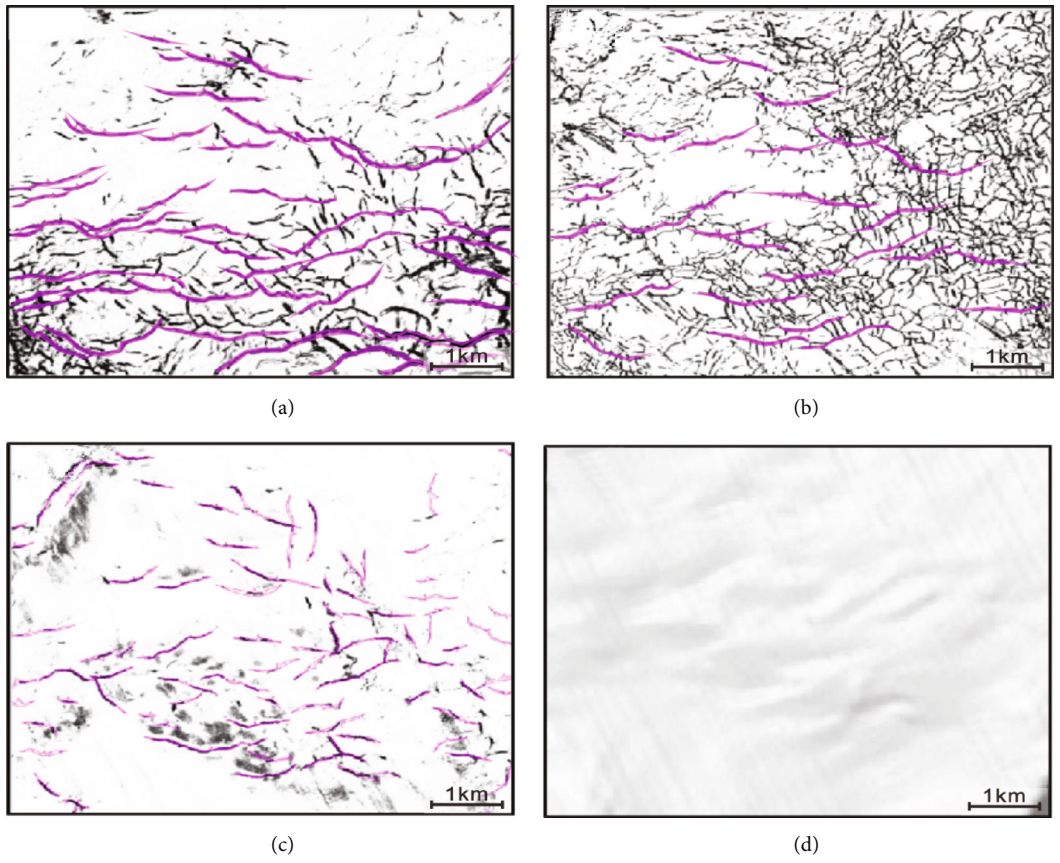

Figure 9: Combination characteristics of strike-slip faults in platform area (purple lines represent strike-slip faults). (a) The coherence attribute slice of the T_{51} stratum (the bottom of the Lingshui I and II group). (b) The coherence attribute slice of the T_3 stratum (the bottom of the Huangliu group). (c) The coherence attribute slice of the T_2 stratum (the bottom of the Yinggehai group). (d) The inclination attribute slice of the T_0 stratum (submarine).

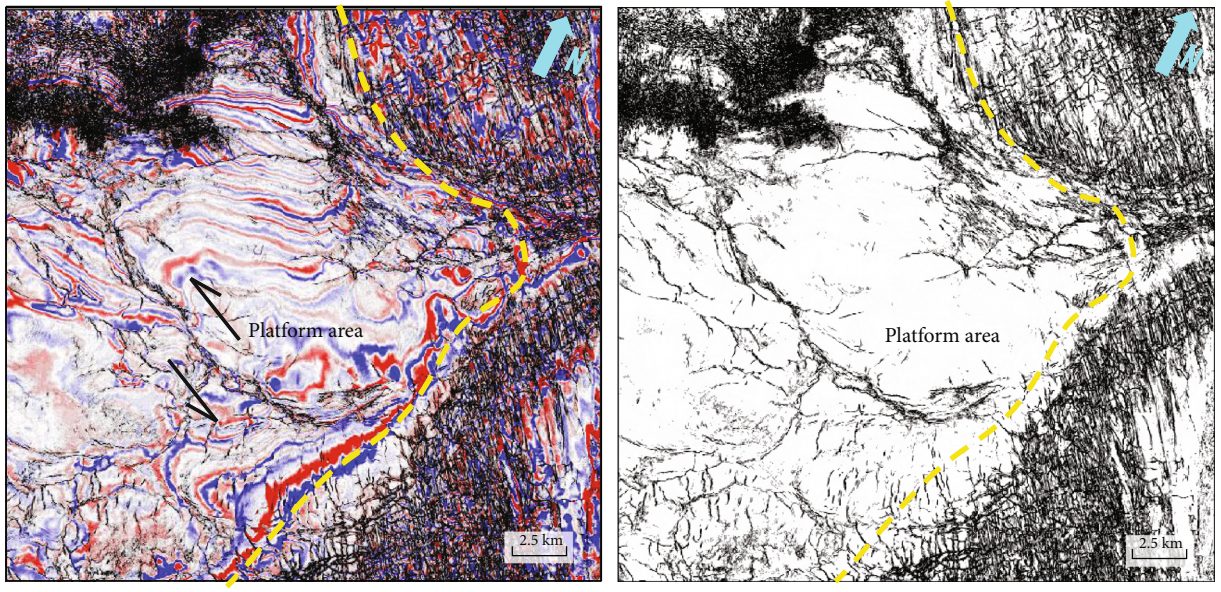

(a) (b)

Figure 10: The characteristics of strike-slip faults during the rift period on the plane. The yellow-dotted line is the geomorphic units' boundary. (a) The profile of 2200 ms time slice from attribute fusion data; black lines indicating faults and fractures, red fillings indicating seismic amplitude troughs, and blue fillings indicating seismic amplitude peaks. (b) The profile of 2200 ms time slice from coherence attribute data; black lines indicating faults and fractures.

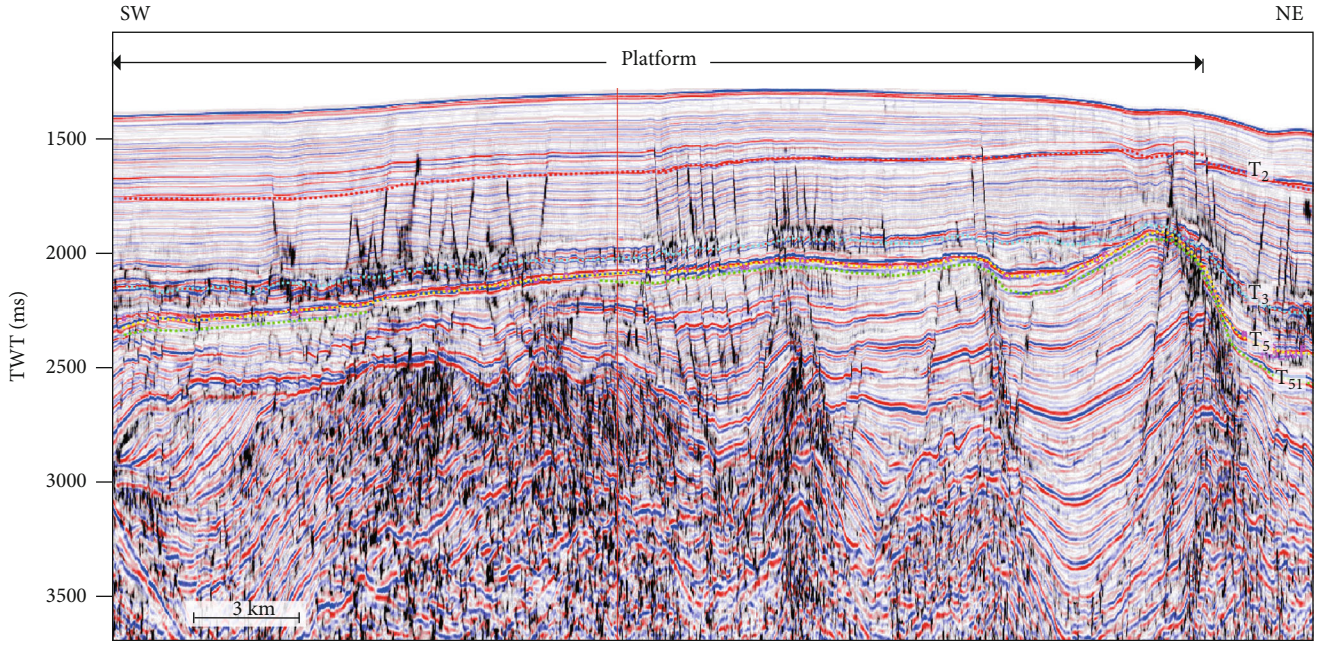

Figure 11: The characteristics of strike-slip faults in attribute fusion data on BB's profile (location on Figure 7).

The normal dip-slip fault system connects the gas source bed of the Lingshui I and II group, the Sanya group, and the Meishan group (T_{51}-T_3) with the GHSZ in the slope area (Figures 7 and 12). It can become a suitable carrier for the vertical migration of hydrocarbons.

The strike-slip fault carrier system connects the two sets of gas source beds with GHSZ in the platform area (Figures 7 and 13). The two sets of gas source beds are the Lingshui III group (T_{52}-T_{51}) and the Lingshui I and II group to the Meishan group (T_{51}-T_3). It can become a suitable carrier for the vertical migration of hydrocarbons.

Generally, the three types of fault systems can play a role in hydrocarbon migration and transportation. However, there are differences in the gas source beds that can be connected and their distribution positions. The polygonal fault system and normal dip-slip fault system are combined to

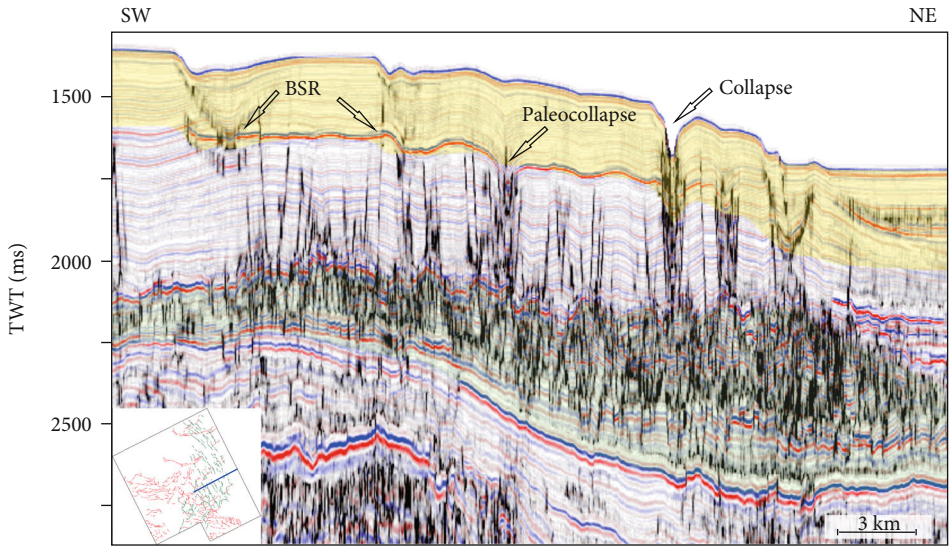

Figure 12: Profile of normal dip-slip fault and polygonal fault carrier system in the slope area. The green filling is the biogas source bed of the Lingshui group I and II to Meishan group (T_{51}-T_3).

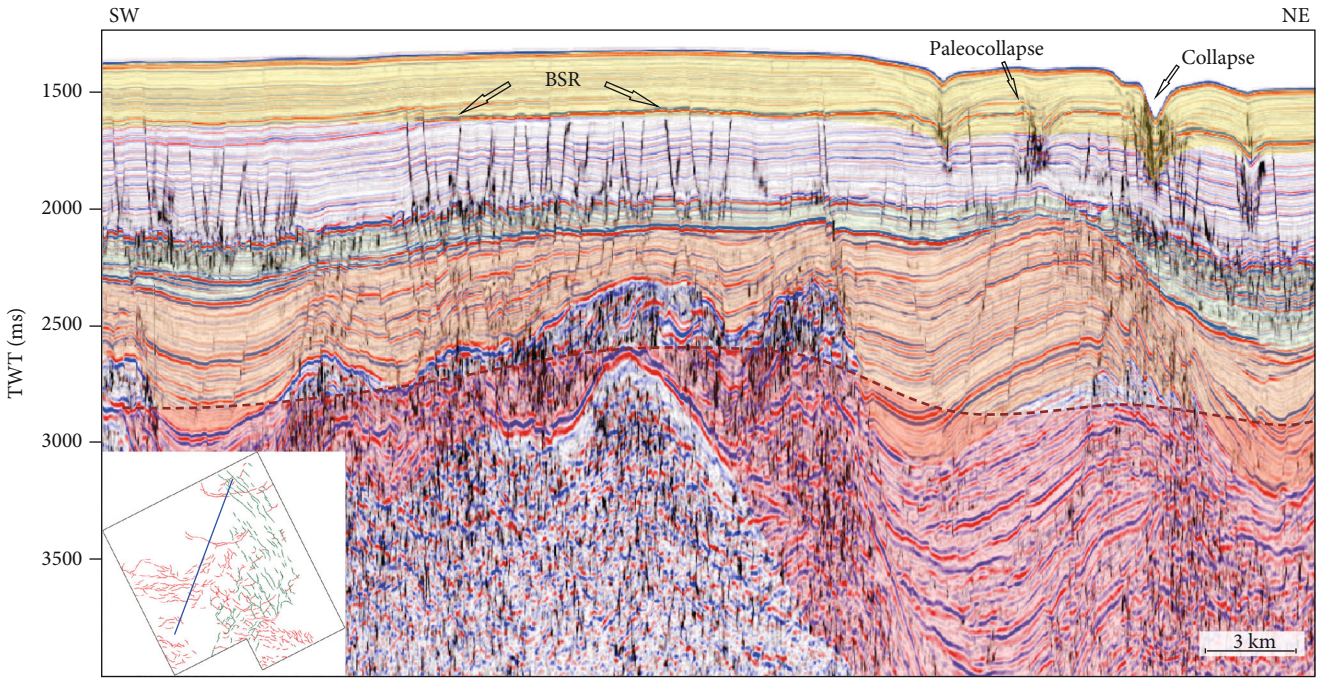

Figure 13: Profile of strike-slip fault carrier system in the platform area. The green filling is the biogas source bed of the Lingshui group I and II to the Meishan group (T_{51}-T_3). Another biogas source bed of the Lingshui III group (T_{52}-T_{51}) is the orange filling. The maturity threshold interface is the red-dotted line. The pyrolysis gas source bed is the red filling.

form a composite fault carrier system, which jointly undertakes the vertical migration of hydrocarbons in a gas source bed in the slope area. The strike-slip fault system mainly undertakes the vertical migration of hydrocarbons in two gas source beds in the platform area.

5.2. The Fitting Analysis of Faulting and Source Timing

5.2.1. The Fault Timing. We speculate that the polygonal fault system is formed in the sedimentation period of Huangliu by its origin mechanism, i.e., 10.5-5.5 Ma. The top of the Lingshui I and II strata is argillaceous limestone sediment with thin layers of limestone. The Sanya strata are mainly bathyal mudstone sediment. The Meishan strata are interbedded sediment with different thicknesses of calcareous mudstone and argillaceous limestone. At the early burial stage, the pore water at the top of the Lingshui I and II strata and the Meishan strata is discharged to the adjacent strata preferentially, which forming an impermeable sealing layer at the top of the Lingshui I and II strata, also at the top

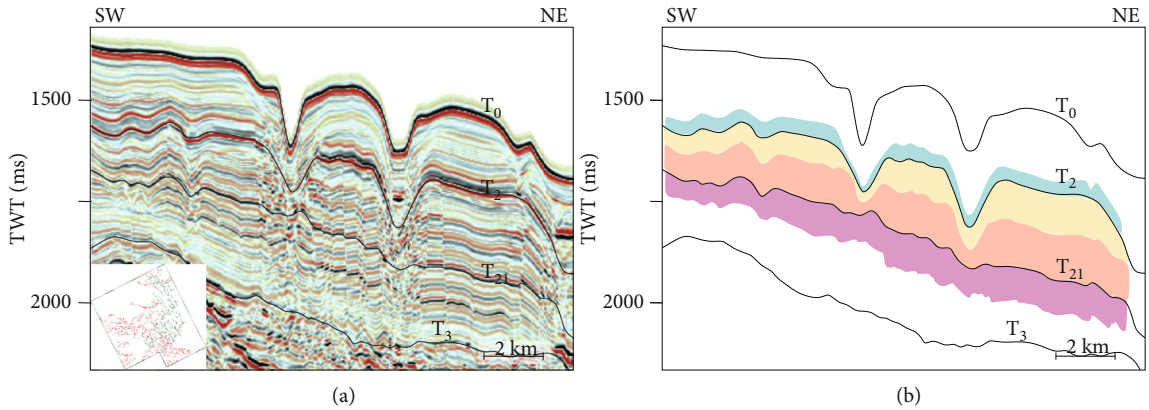

Figure 14: (a) Profile of the normal dip-slip fault system in the slope area. (b) The interpretation of growth strata. The yellow- and red-filled strata are characterized by downward thickening. The downward thickening rate of the yellow-filled strata is greater than that of red-filled formation strata. The green- and pink-filled strata have no obvious change in thickness. It indicates that the fault activity occurred after the deposition of the pink formation and before the deposition of the green formation, that is, the Huangliu II group.

of the Meishan strata. With the depositing of the Huangliu strata, the pore water in the Sanya and the Meishan strata is blocked in the pores, and the strata are undercompacted. As there is more pore water in the Sanya and the Meishan strata, the density is less than that of the overlying strata. The pore water blocked in the strata is in an overpressure state with the deposit continuously. Hydraulic fractures and faults are generated at the top of the overpressure layer to release the pressure, forming a phase polygonal fault limited from the Lingshui I and II group to the Meishan group. The deep hydrocarbon fluid continues to migrate upward with the overlaying strata depositing, causing the overpressure accumulation inside the polygonal fault array again and then forming a new polygonal fault array in the Meishan group. The study area shows that the density of the polygonal fault array increases upward.

It is speculated that the normal dip-slip fault system was formed in the sedimentation period of Huangliu, i.e., 8.2-5.5 Ma. The growth strata are deposited in the ridge and flank of the anticline during the tectonic deformation period. It belongs to the sedimentation during the syntectonic period and records the characteristics of tectonic activities, such as the deformation style, deformation time, and deformation mechanism of the structure [76–78]. As a result of uplift activity, the slope area is stretched, causing the hanging wall slides. The accommodation space generated by the downward propagation of faults is filled by the growth strata, which is shown as downward thickening characteristics (Figure 14). The upper part of the Huangliu group (yellow- and red-filled strata) has the characteristics of downward thickening, while the lower part of the Huangliu group (pink-filled strata) has no obvious thickness change, which is shown as the characteristic of pregrowth strata [79]. The lower part of the Yinggehai group (green-filled strata) has no obvious thickness change, which is shown as the characteristics of postgrowth strata. Therefore, we considered that the normal dip-slip fault was formed in the late stage of the Huangliu sedimentation.

The strike-slip faults started to move from the late Oligocene, with episodic activity characteristics. This paper focuses on the activity time analysis in the regional subsidence period. The late compression property of the strike-slip fault has led to local fold deformation in the study area. The thickness of the growth strata is thinner towards the anticline ridge in the Yinggehai group (Figure 15). The tip of the growth strata wedge points to the anticline ridge. Angular unconformity hosts in the growth strata, and its surface develops on the flank close to the anticline ridge. The angle unconformity gradually becomes conformity as is far away from the anticline ridge. Taking the activity period of the Honghe strike-slip fault system into consideration [47–49, 75], the fault array occurred once in the early sedimentation stage of the Yinggehai group, i.e., 5.5-3 Ma. At present, the seabed with the characteristics of sediment drapes indicates that the strike-slip activity is still continuous (Figure 8(d)).

5.2.2. The Fitting Analysis of Faulting and Hydrocarbon Generating. The composite fault carrier system, which is composed of a polygonal fault system (10.5-5.5 Ma) and a normal dip-slip fault system (8.2-5.5 Ma), was active before the peak hydrocarbon generation (5 Ma) which is the formation time of the Lingshui I and II group to the Huangliu group. That is, during the period of massive hydrocarbon expulsion from the strata, the polygonal fault has been formed and has increased the vertical and lateral connectivity of transition strata. In situ hydrocarbons had accumulated in the polygonal fault system. At the same time, hydrocarbons in the rifting strata migrate upward through deep faults to the polygonal fault system. This behavior makes the transition strata become gas-rich strata, which reserves sufficient gas sources for NGH accumulation in the overlying Yinggehai group. The normal dip-slip fault system migrated hydrocarbons enriched in the transition strata and the Huangliu group to the GHSZ.

The strike-slip fault carrier system has been active once in the early stage (5.5-3 Ma) of Yinggehai sedimentation

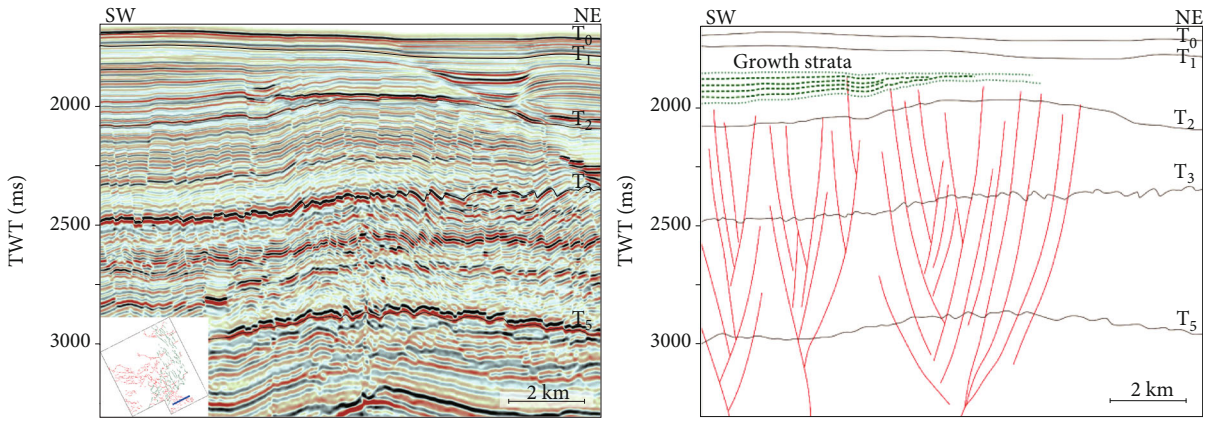

Figure 15: (a) Profile of strike-slip fault system in the trough area. (b) The interpretation of growth strata related to the strike-slip fault. The red lines indicate the strike-slip faults, and the green lines are the growth strata. Green-dotted lines are the internal interpretation of growth strata, which is characterized by onlap.

and is still weakly active now. The strike-slip activity occurred after the peak hydrocarbon generation of the Lingshui group to the Meishan group formation time (at about 8-5 Ma). The hydrocarbons that have accumulated in the rift strata and transition strata can migrate to the GHSZ along with this fault system. The thinness of the Lingshui I and II group to the Meishan group is too thin to contribute valuable gas in the platform area, while the Lingshui III group contributes more.

5.3. Migration Performance of the Fault Carrier System. The comprehensive migration performance of the two fault carrier systems in the study area is mainly affected by four factors: fault zone width, extension length, distance, and density. In this study, the fault migration coefficient R is calculated according to the four factor parameters to compare the two fault carrier systems [80–84].

$$R = \frac{1}{S}\sum_{j=1}^{n} D_j H_j \sin\theta. \quad (1)$$

In the formula, R is the transport coefficient of the fault carrier system; H_j is the fault distance, km; D_j is the hydraulic radius, $D_j = A_j \div C_j$, km; A_j is the cross-section area of hydrocarbon passing through the fault zone, $A_j = T_j L_j$, km^2; C_j is the perimeter of the section, $C_j = 2(T_j + L_j)$, km; T_j is the width of the fault zone, $T_j = 0.62H_j^{0.875}$ [85], km; L_j is the fracture extension length, km; θ is the fault dip angle, °; S is the plane distribution range of the study area, km^2; n is the number of fractures connecting the gas layer. The structural dip angle (θ) and fault distance (H_j) can be obtained from the structural plane; the extension length (L_j), the number of fractures (n), and the distribution range of the study area (S) can be obtained from the coherent attribute data by using the system parameter tools. By the statistical samples of the faults that can reach the bottom of the GHSZ, we calculated the migration coefficients of the two types of dominant fault carrier systems (Table 1).

Table 1: Evaluation of carrier system migration performance in the study area.

Parameters	Composite fault carrier system	Strike-slip fault carrier system
Dip angle (°)	34~70	38~57
Density (pieces/km)	1.6 ~ 2.9	1.2 ~ 1.8
Distance (m)	7 ~ 18	12~13
Extension length (km)	0.2 ~ 0.9	0.5 ~ 3.5
R ()	14.55	10.07

The calculation results show that the migration performance of the composite fault carrier system is better than that of the strike-slip fault carrier system.

5.4. The Evaluation of Fault Carrier Systems. The evaluation of fault carrier systems and the prediction of favorable zones are the ultimate goal of studying the carrier systems. We can accurately predict favorable exploration zones by determining the dominant fault carrier systems by considering the geological characteristics of hydrate accumulation in the basin. Based on the above three factors, (a) it connects the gas source bed and the GHSZ. (b) Its activity time is well consistent with the peak hydrocarbon generation of the gas source bed. And these hydrocarbons can be accumulated and deposited. (c) During the hydrocarbon migration period, the migration capacity is good [86, 87], and we evaluated the role of the fault carrier system in the hydrocarbon migration and NGH accumulation, then established fault carrier patterns and finally predicted favorable zones.

5.4.1. The Role of Fault Carrier Systems in Hydrocarbon Migration and NGH Accumulation

(1) The Pattern of the Composite Fault Carrier System. The composite fault carrier system (polygonal and normal dip-

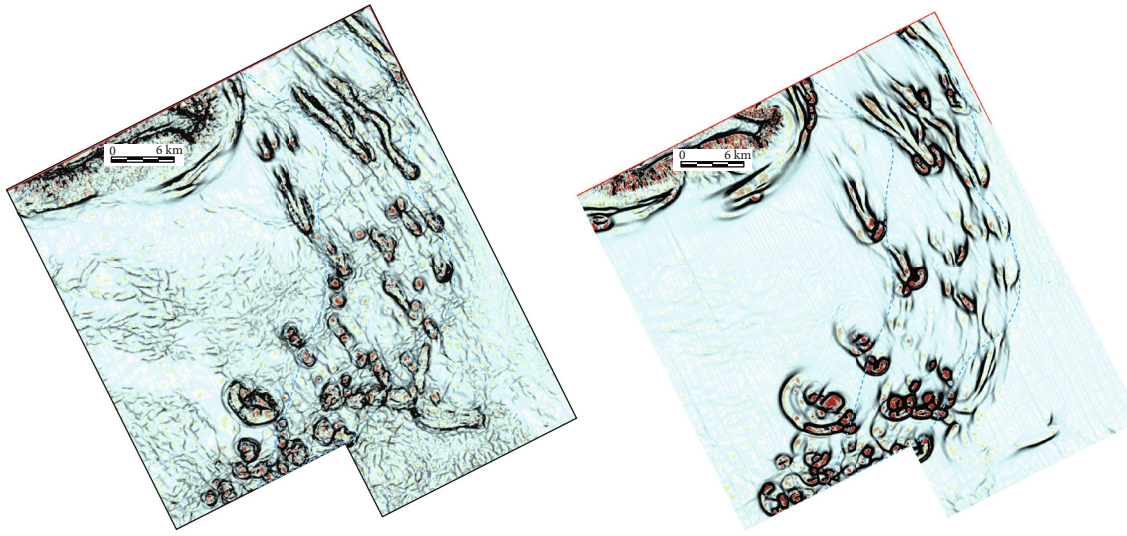

(a) (b)

Figure 16: Slices of curvature attribute data along with a layer: (a) the curvature attribute slice of T_2 (the bottom of the Yinggehai group); (b) the curvature attribute slice of T_0 (submarine). The black fillings in the profile are a positive curvature value, the red fillings are a negative curvature value, and the white fillings are a 0 value. The edge of the collapse structure is a positive curvature value. The interior of the collapse structure is a negative curvature value. The blue-dotted line is the boundary of the geomorphic units in regional subsidence strata.

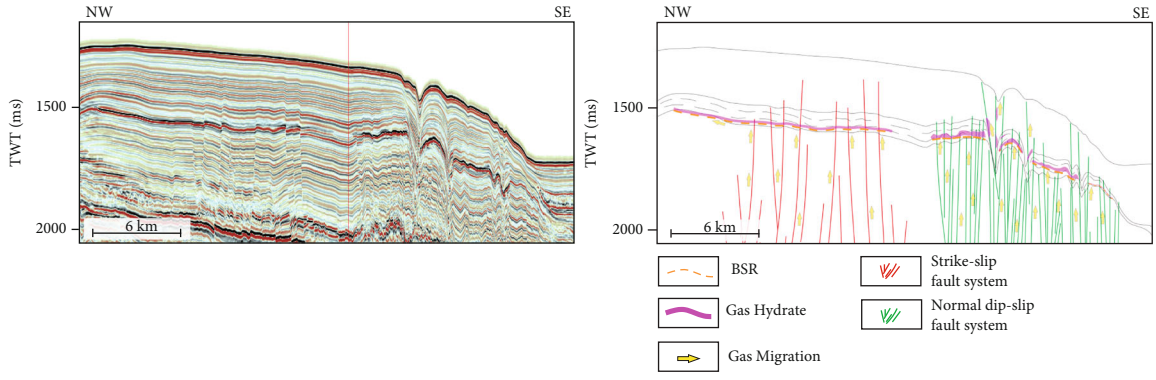

(a) (b)

Figure 17: (a) Profile of two fault carrier systems with BSR. (b) The pattern of two fault carrier systems with NGH accumulation.

slip fault carrier system) pattern leads to hydrocarbon leakage or accumulation. The polygonal fault system with a high fault density has many hydrocarbon migration paths, resulting in fast fluid flowing and strong fault transportation ability. The normal dip-slip fault system has a large fault distance, a higher degree of a fracture network in the fault zone, and provides an adequate migration space for vertical hydrocarbon migration. So the hydrocarbon migration flux per unit of time is considerable, illustrating the migration capacity of these faults is strong. The activity period of the composite fault carrier system is well consistent with the peak hydrocarbon generation of the Lingshui group to the Meishan group, which makes hydrocarbons accumulated in the transition strata migrate upward rapidly. An extensive fluid migration is the main reason for ancient collapse structures at the bottom of the Yinggehai group in the slope area (Figure 12). Most of these paleocollapse structures are arranged in the NW-SE trend to form a collapsed chain (Figure 16(a)). The strike of the collapsed chain is consistent with that of the normal dip-slip fault system, indicating that this fault carrier system has an intense migration capacity at that time. After the fault activity stopped (after 5.5 Ma), the overlying mudstone caprock of the bathyal sediment gradually deposited, and the gas source bed enters the high hydrocarbon generation stage. Hydrocarbons can migrate upward along the fault to the GHSZ zone and accumulated in reservoirs (Figures 17(a) and 17(b)). The current strike-slip activity will reactivate the polygonal and normal dip-slip fault system, causing hydrocarbon to migrate upward along these faults, and resulting in seabed fluid flowing. The current seabed collapse structures are easy to occur at the intersection of the strike-slip fault system and normal dip-slip fault system (Figures 16(b) and 18), indicating that the composite fault carrier system still maintains intense transport capacity. Unfortunately, hydrocarbons preferentially escape to the seabed, which will destroy the formed gas hydrate deposits. It

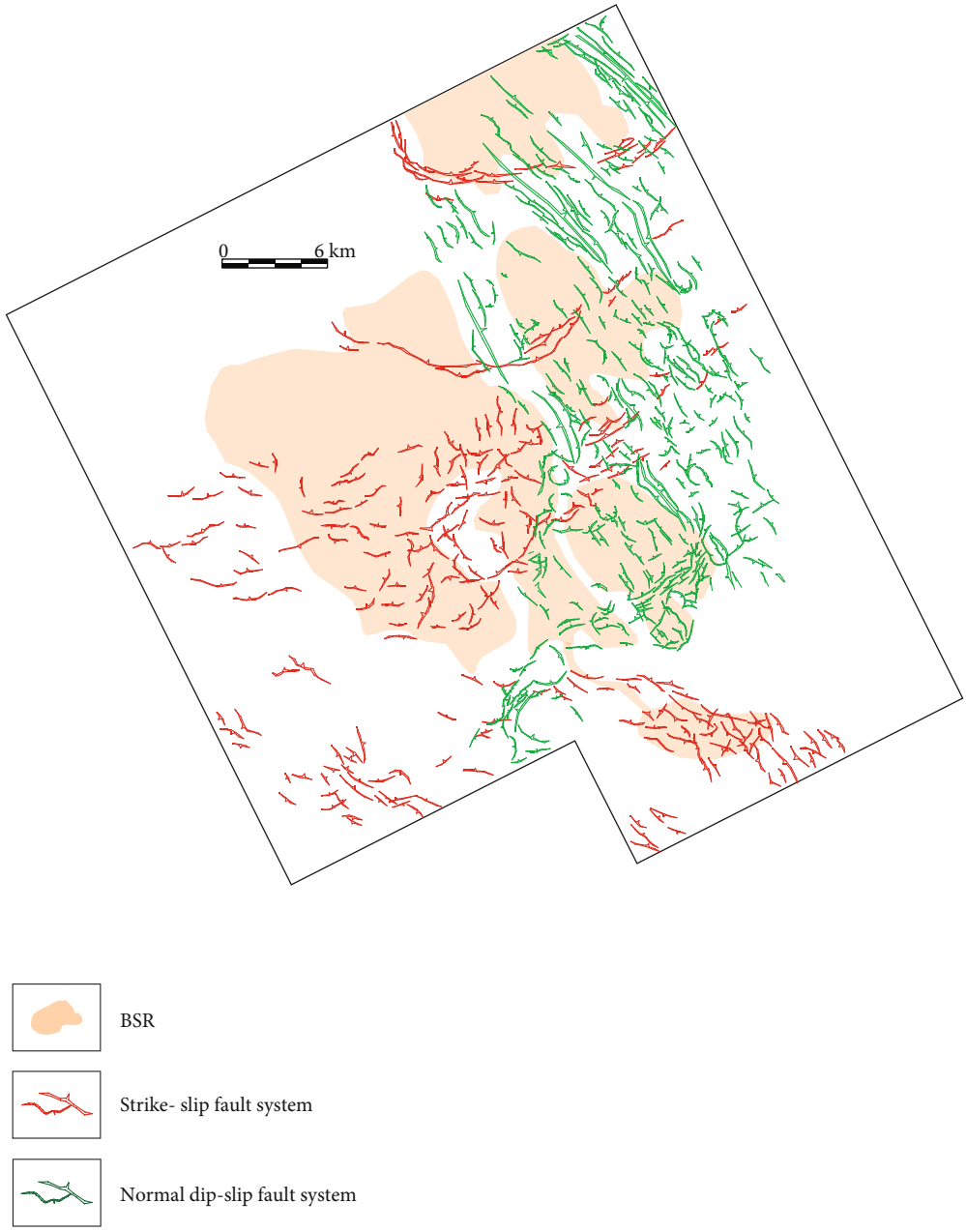

Figure 18: Distribution characteristics of BSR and two types of fault carrier systems through GHSZ in the study area.

caused the discontinuous distribution of BSR in the slope area (Figures 17(b) and 18). Hydrocarbons preferentially escape to the seabed in the vicinity of the leakage channel, which will lead to the formation of massive and vein NGH in fractures (Figure 17(b)). The composite fault carrier system in the nonleakage area is the dominant fault carrier system, which will lead to the accumulation of pore-filling NGH in the GHSZ. BSR in slope area and its overlying seismic event show stronger amplitude than that in platform area, which may represent higher gas hydrate saturation in this area (Figure 17(a)).

(2) The Pattern of the Strike-Slip Fault Carrier System. The pattern of the strike-slip fault carrier system completes the long-distance and large-scale hydrocarbon migration, which is conducive to the accumulation and deposition of NGH. Although the gas source bed of the Lingshui III group is far from the GHSZ, the strike-slip fault system has characterized by staged activity and well-vertical connectivity. The gas production intensity of the Lingshui III group is the largest, which is conducive to the long-distance migration of hydrocarbons. The strike-slip fault carrier system has a significant extension length in trend, which makes the fracture network in the fault zone wide and the hydrocarbon migration flux large. The strike-slip fault carrier system moved after the peak hydrocarbon generation of the Lingshui III group and has been active until now. Nevertheless, the compressive properties of the fault array are not

conducive to the rapid migration of hydrocarbons to seabed leakage (diapirs mainly cause the collapse structures in the platform area) (Figure 17(b)). Hydrocarbons can slowly migrate into the GHSZ and stably accumulate to form NGH reservoirs (Figure 16(b)). As a result, pore-filling gas NGH may be formed. The strike-slip fault carrier system is the dominant fault carrier system in the study area. The distribution of the BSR (Figure 17) clearly shows its widespread occurrence throughout the study area, with the most continuous BSR occurring within the platform area.

5.4.2. Prediction for Favorable Exploration Zones. Based on the above, there are apparent differences between the two types of fault carrier systems in the "source to the zone" system, distribution position, migration performance, and carrier pattern. The strike-slip fault carrier system shows a reservoir forming mode of remote and vertical, a single type of mineral deposit, and effective transport. The composite fault carrier system shows the near-source and vertical reservoir forming mode, multiple types of mineral deposits, and efficient transportation. Their distribution location, transport patterns, and migration performance have affected the reservoir forming behavior of NGH.

The strike-slip fault carrier system is formed under the background of regional strike-slip activities, and it can connect long-distance and high-quality gas source beds in a vertical direction. This type of fault carrier system can complete the effective reservoir formation of long-distance migration, large-area accumulation, and single-filling type hydrocarbons. Hydrocarbons migrate vertically along the compressive active faults to the GHSZ and fill in the sediment pores of the reservoir, and its distribution area is a preferential zone of the fault carrier system in the study area.

The composite fault carrier system is influenced by the tectonic uplift caused by regional strike-slip activities. It can connect the main gas source layer at a short distance vertically. Hydrocarbons migrate vertically along the extensional active fault to the GHSZ and fill in the pores of the reservoir or the fractures of the leakage channel. This kind of fault carrier system can complete the highly efficient accumulation of NGH in short-distance migration, scattered accumulation, and multifilling types. The leakage passage is the priority path of hydrocarbon migration, which will affect the total amount of hydrocarbon accumulation. So the distribution area of the composite fault carrier system is a second favorable zone of the fault carrier system in the study area.

6. Conclusion

(i) Two fault carrier systems are formed in the study area. The composite fault carrier system is composed of "density inversion" polygonal faults host in transition strata and normal dip-slip faults host in regional subsidence strata. The strike-slip fault carrier system comprises strike-slip faults that have been active for a long time since the rift stage. The formation of the two types of fault systems is closely related to the activity of the Honghe-Yinggehai strike-slip fault in the western South China Sea

(ii) The strike-slip fault carrier system is a reservoir forming mode with a far source, vertical migration, a single type of mineral deposition, and adequate transportation, which is a preferential fault carrier system. The composite fault carrier system shows a reservoir forming mode of near-source, vertical migration, multiple types of mineral deposition, and efficient transportation, which is a second favorable fault carrier system

(iii) In this paper, a new evaluation method for the NGH fault carrier system is proposed, including the connection between fault and "source to zone", the coincidence between faulting time and the peak hydrocarbon generation, and the fault migration performance. This work uses this evaluation method to establish a migration model and predict favorable zones. This research provides ideas and sample support for establishing evaluation criteria of fault carrier systems in the NGH occurrence area of the northern South China Sea and has guiding significance for the NGH favorable exploration areas

Data Availability

The data used to support the findings of this study are included within the article.

Conflicts of Interest

The authors declare no conflict of interest.

Authors' Contributions

L.H. was responsible for the conceptualization of the study, P.L. was in charge of the methodology, X.C. administered the software, S.M. conducted the formal analysis and the writing of original draft preparation, Q.M. managed the investigation, and G.H was responsible of the writing, review, and editing of the manuscript. All authors have read and agreed to the published version of the manuscript.

Acknowledgments

We wish to thank Dr. Tao Li for editorial assistance. This research was funded by the National Natural Science Foundation of China (No. 41472097).

References

[1] E. D. Sloan, *Clathrate Hydrates of Natural Gases*, J. Marcel Dekker, New York, 1991.

[2] N.-Y. Wu, J.-Q. Liang, H.-B. Wang et al., "Marine gas hydrate system: State of the Art," *Journal of Geosciences*, vol. 22, no. 3, pp. 817–828, 2008.

[3] Y.-H. Gong, S.-X. Yang, H.-B. Wang, J.-Q. Liang, and J. Liang, "Prospect of gas hydrate resources in Qiong Dongnan Basin,"

Journal of Jilin University(Earth Science Edition), vol. 48, pp. 1030–1042, 2018.

[4] P.-B. Su, Z.-B. Sha, S.-Y. Chang, J.-Q. Liang, and S.-Y. Fu, "Geological models of gas hydrate formation in the eastern sea area of the Pearl River Mouth Basin," *Natural Gas Industry*, vol. 34, pp. 162–168, 2014.

[5] X.-J. Wang, S.-G. Wu, D.-D. Dong, Y.-Q. Guo, and D. Hutchinson, "Control of mass transport deposits over the occurrence of gas hydrate in Qiongdongnan Basin," *Marine Geology & Quaternary Geology*, vol. 31, no. 1, pp. 109–118, 2011.

[6] J. Liang, M.-J. Wang, J.-A. Lu, H.-B. Wang, J.-Q. Liang, and P.-B. Su, "Logging R characteristics of gas hydrate formation in Shenhu area of South Shina Sea," *Journal of Geosciences*, vol. 24, pp. 506–514, 2010.

[7] X. Huang, Y.-H. Zhu, Z.-Q. Lu, and P.-K. Wang, "Study on genetic types of hydrocarbon gases from the gas hydrate drilling area, the northern south sea," *Journal of Geosciences*, vol. 24, pp. 576–580, 2010.

[8] W. Zhang, J.-Q. Liang, J.-X. He et al., "Differences in natural gas hydrate migration and accumulation between GMGS1 and GMGS3 drilling areas in the Shenhu area, northern South China Sea," *Natural Gas Industry*, vol. 38, pp. 138–149, 2018.

[9] W. Zhang, J.-Q. Liang, P.-B. Su et al., "Migration pathways of hydrocarbons and their controlling effects associated with high saturation gas hydrate in Shenhu area, northern South China Sea," *Geology in China*, vol. 45, pp. 1–14, 2018.

[10] J.-F. Li, J.-L. Ye, X.-W. Qin et al., "The first offshore natural gas hydrate production test in South China Sea," *China Geology*, vol. 1, no. 1, pp. 5–16, 2018.

[11] S.-W. Zhou, J.-Z. Zhao, Q.-P. Li et al., "Optimal design of the engineering parameters for the first global trial production of marine natural gas hydrates through solid fluidization," *Natural Gas Industry B*, vol. 5, pp. 118–131, 2017.

[12] S.-W. Zhou, W. Chen, and Q.-P. Li, "Research on the solid fluidization well testing and production for shallow non-diagenetic natural gas hydrate in deep water area," *China Offshore Oil Gas*, vol. 29, pp. 1–8, 2017.

[13] J.-L. Ye, X.-W. Qin, and W.-W. Xie, "Main progress of the second gas hydrate trial production in the South China Sea," *Geology in China*, vol. 47, pp. 557–568, 2020.

[14] Ministry of Land and Resources of the People's Republic of China, *China Mineral Resources*, 2020.

[15] T. S. Collett, "Gas hydrate petroleum systems in marine and arctic permafrost environments," *Gcssepm Proceedings*, vol. 29, pp. 6–30, 2009.

[16] G. M. Ingram, T. J. Chisholm, C. J. Grant, C. A. Hedlund, P. Stuart-Smith, and J. Teasdale, "Deepwater North West Borneo: hydrocarbon accumulation in an active fold and thrust belt," *Marine and Petroleum Geology*, vol. 7, pp. 879–887, 2004.

[17] J. Hauschildt, J. Vogt, and V. Unnithan, "Methane hydrate and two-dimensional fluid transport model: comparison with Blake Ridge chlorinity measurements," *Transport in Porous Media*, vol. 3, pp. 425–440, 2013.

[18] A. M. Trehu and O. Leg, "An Introduction to ODP Leg 204: Drilling Gas Hydrate on Hydrate Ridge," in *EGS-AGU-EUG Joint Assembly*, 2003.

[19] C. Lopez, G. Spence, R. Hyndman, and D. Kelley, "Frontal ridge slope failure at the northern Cascadia margin: margin - normal fault and gas hydrate control," *Journal of Geology*, vol. 11, pp. 967–970, 2010.

[20] R. Boswell, T. S. Collett, M. Frye, W. Shedd, D. R. McConnell, and D. Shelander, "Subsurface gas hydrates in the northern Gulf of Mexico," *Marine and Petroleum Geology*, vol. 1, pp. 4–30, 2012.

[21] M. Riedel, A. M. Tréhu, and G. D. Spence, "Characterizing the thermal regime of cold vents at the northern Cascadia margin from bottom-simulating reflector distributions, heat-probe measurements and borehole temperature data," *Marine Geophysical Researches*, vol. 1-2, pp. 1–16, 2010.

[22] K. Baba, "BSRs and associated reflections as an indicator of gas hydrate and free gas accumulation: an example of accretionary prism and forearc basin system along the nankai trough, off Central Japan," *Resource Geology*, vol. 1, pp. 11–24, 2004.

[23] G. Y. Dong, N. K. Kang, B. Y. Yi et al., "Occurrence and seismic characteristics of gas hydrate in the Ulleung Basin, East Sea," *Marine and Petroleum Geology*, vol. 11, pp. 236–247, 2013.

[24] S. Horozal, G. H. Lee, B. Y. Yi et al., "Seismic indicators of gas hydrate and associated gas in the Ulleung Basin, East Sea (Japan Sea) and implications of heat flows derived from depths of the bottom-simulating reflector," *Marine Geology*, vol. 258, no. 1-4, pp. 126–138, 2009.

[25] Z. B. Sha, J. Q. Liang, and P. B. Su, "Natural gas hydrate accumulation and drilling results analysis in the eastern part of the Pearl River Mouth Basin," *Earth science frontiers*, vol. 22, no. 6, pp. 125–135, 2015.

[26] W. Zhang, J. Q. Liang, J. X. He et al., "Differences in natural gas hydrate migration and accumulationbetween GMGS1 and GMGS3 drilling areas in the Shenhu area, northern South China Sea," *Natural Gas Industry*, vol. 38, no. 3, pp. 138–149, 2018.

[27] P.-B. Su, J.-Q. Liang, S.-Y. Fu, W.-Y. Lv, and Y.-H. Gong, "Geological background and accumulation models of gas hydrate reservior in northern South China," *Geology in China*, vol. 44, pp. 415–427, 2017.

[28] N. Qiu, Z.-W. Wang, Z.-F. Wang, Z.-P. Sun, Z. Sun, and D. Zhou, "Tectonostratigraphic structure and crustal extension of the Qiongdongnan Basin, northern South China Sea," *Chinese Journal of Geophysics*, vol. 57, pp. 3189–3207, 2014.

[29] B.-C. Yao, L. Wan, and N.-Y. Wu, "Cenozoic plate tectonic activities in the great South China Sea area," *Geology in China*, vol. 31, pp. 113–122, 2004.

[30] B.-C. Yao, L. Wan, and Z.-H. Liu, "Tectonic dynamics of cenozoic sedimentary basins and hydrocarbon resources in the South China Sea," *Earth Science*, vol. 29, pp. 543–549, 2004.

[31] G.-C. Zhang, X.-J. Xie, and W.-Y. Wang, "Tectonic types of petroliferous basins and its exploration potential in the South China Sea," *Acta Petrolei Sinica*, vol. 34, pp. 611–627, 2013.

[32] B.-C. Yao, "Tectonic evolution of the South China Sea in Cenozoic," *Marine Geology and Quaternary Geology*, vol. 16, pp. 1–13, 1995.

[33] H.-F. Gao, Y.-T. Wang, and L.-H. Guo, "Petroleum geological conditions and prospects in the Zhongjiannan basin in the western South China Sea," *Geology in China*, vol. 34, no. 4, pp. 592–598, 2007.

[34] H.-F. Gao, X.-H. Zeng, Z.-H. Liu, and Z.-L. Bai, "Simulating of subsidence history and analysis of tectonic evolutionary characteristics of Liyue Basin in the South China Sea," *Geotectonica et Metallogenia*, vol. 29, pp. 385–390, 2005.

[35] G.-C. Zhang, "Tectonic evolution of deepwater area of northern continental margin in South China Sea," *Acta Petrolei Sinica*, vol. 31, pp. 528–541, 2010.

[36] Z. Sun, Z.-X. Zhao, J.-B. Li, D. Zhou, and Z.-W. Wang, "Tectonic analysis of the breakup and collision unconformities in the Nansha," *Chinese Journal of Geophysics*, vol. 54, pp. 3196–3209, 2011.

[37] X.-N. Xie, J.-Y. Ren, Z.-F. Wang, X.-S. Li, and C. Lei, "Difference of tectonic evolution of continental marginal basins of South China Sea and relationship with SCS spreading," *Earth Science Frontiers*, vol. 22, pp. 77–87, 2015.

[38] H. Yi, G.-J. Zhong, and J.-F. Ma, "Fracture characteristics and basin evolution of the Taixinan Basin in Cenozoic," *Petroleum Geology and Experiment*, vol. 29, pp. 560–564, 2007.

[39] X.-X. Li and G.-H. Zhu, "The fault system and its hydrocarbon carrier significance in Qiongdongnan basin," *China Offshore Oil and Gas*, vol. 17, pp. 1–7, 2005.

[40] G.-J. Zhong, L.-Y. Wu, Z. Lin, Y.-J. Yao, and H. Yi, "Characteristics of faults on the northeastern continencal slope of the South China Sea and their controls on basin evolution," *Geology in China*, vol. 35, pp. 456–462, 2008.

[41] B.-L. Lu, P.-J. Wang, G.-C. Zhang, and W.-Y. Wang, "Characteristic of regional fractures in South China Sea and its basement tectonic framework," *Progress in Geophysics*, vol. 30, pp. 1544–1553, 2015.

[42] L. Duan, J.-X. Pei, Y.-Z. Zhang et al., "Tectonic characteristics of extensional datachment basin in southern South China Sea," *Marine Origin Petroleum Geology*, vol. 23, pp. 71–80, 2018.

[43] X.-J. Wu, X. Pang, M. He, J. Shen, and C.-Z. Yan, "Structural style and dynamical mechanism during rifting in the passive-continental-margin basins, the northern South China Sea," *China Offshore Oil and Gas*, vol. 26, pp. 43–50, 2014.

[44] C. Zhang, S.-M. Wu, and X.-L. Qiu, "Formation of foreland basins in the south of the South China Sea," *Marine Geology & Quaternary Geology*, vol. 27, pp. 61–70, 2007.

[45] D.-H. Yang, H.-M. Tong, C.-W. Fan, K.-Z. Xiao, and C.-Y. Wang, "Determination of the tectonic transformation surface in Yinggehai Basin and its geological significance," *Geotectonica et Metallogenia*, vol. 43, pp. 590–602, 2019.

[46] C.-S. Lin, J.-Y. Gao, X.-J. Yu, F. Ye, and Y.-H. Tan, "Characteristics of tectonic movement in the northern of South China Sea during the Cenozoic," *Acta Oceanologica Sinica*, vol. 28, pp. 81–86, 2006.

[47] J.-L. Sun, H.-L. Xu, and Y.-M. Li, "Neotectonics in the northeastern South China Sea and its dynamic mechanism," *Marine Geology & Quaternary Geology*, vol. 29, pp. 61–68, 2009.

[48] D.-W. Wang, S.-G. Wu, C.-F. Li, and G.-S. Yao, "Submarine slide evidence for late Miocene strike-slip reversal of the Red River Fault," *Science China Earth Sciences*, vol. 46, pp. 1349–1357, 2016.

[49] C. Lei, J.-Y. Ren, J.-X. Pei et al., "Tectonics of the offshore Red River fault: implication of the junction of the Yinggehai and Qiongdongnan Basins," *Science China Earth Sciences*, vol. 51, pp. 1349–1357, 2021.

[50] A. Q. Li, Q. Ye, Z. Wang, M. Li, and K. Chen, "Sedimentary characteristics andsignificance in hydrocarbon exploration of sandy debris flow in Meishan Formation of the northern Lingshui sag, Qiongdongnan Basin," *Bulletin of Geological Science and Technology*, vol. 40, no. 1, pp. 110–118, 2021.

[51] P. F. Xiong, T. Jiang, Z. G. Kuang, C. Cheng, J. Ren, and H. Lai, "Sedimentary characteristics and origin of moundes in Meishan Formation, southern Qiongdongnan Basin," *Bulletin of Geological Science and Technology*, vol. 40, no. 4, pp. 11–21, 2021.

[52] J.-P. Liu, X.-L. Jian, H.-J. Wang, L.-L. Wang, G.-Y. Wang, and G. Cheng, "Thermal evolution history of hydrocarbon source rock in the Zhongjiannan Basin, western South China Sea," *Journal of Geosciences*, vol. 44, pp. 737–741, 2020.

[53] C. Y. Sun, N.-y. Wu, B.-h. Ni, and S. Yan, "Geochemical characteristics of gaseous hydrocarbons and hydrate resource prediction in the Qiongdongnan Basin of the South China Sea," *Journal of Geosciences*, vol. 21, no. 1, pp. 95–100, 2007.

[54] Y. H. Huang, Z. Liu, F. L. Lv, Y. Wu, and X. S. He, "Early prediction on source rocks of the Oligocene Yacheng formation in the deepwater area of Huaguang Depression, Qiongdongnan Basin," *Acta Geologica Sinica*, vol. 89, no. 4, pp. 805–816, 2015.

[55] J. X. He, B. Xia, Q. M. Zhang, S. L. Zhang, and B. M. Liu, "Resources base and exploration of biogenic and sub-biogenic gas in marginal basin of the northern South China Sea," *Natural Gas Geoscience*, vol. 16, no. 2, pp. 167–174, 2005.

[56] J. Liu, R. Yang, J. H. Zhang, W. Wei, and D. Wu, "Gas hydrate accumulation conditions in the Huaguang Depression of Qiongdongnan Basin and prediction of favorable zones," *Marine Geology & Quaternary Geology*, vol. 39, no. 1, pp. 134–142, 2018.

[57] Z. Q. Yang, W. Zhou, Y. Wang et al., "Subdivision of the first member of Huangliu formation in Dongfang area of Yinggehai Basin and the main factors controlling the sedimentary evolution of submarine fan," *China Offshore Oil and Gas*, vol. 34, no. 1, pp. 55–65, 2022.

[58] J. X. Pei, C. Zhang, W. Kang, L. Juan, and W. Shaokai, "Tectonic evolution and depositional response in southern continental marginal basins of South China Sea during period of rift- drift-foreland: a case study from the Liyue Basin," *Bulletin of Geological Science and Technology*, vol. 40, no. 2, pp. 42–53, 2021.

[59] M. Su, R. Yang, N. Y. Wu et al., "Structural characteristics in the Shenhu area, northern continental slope of South China Sea, and their influence on gas hydrate," *Acta Geologica Sinica*, vol. 88, no. 3, pp. 318–326, 2014.

[60] X. Xu, Y. M. Li, X. H. Luo, X. B. Shi, and X. Q. Yang, "Comparison of different-type heat flows at typical sites in natural gas hydrate exploration area on the northern slope of the South China Sea," *Chinese Journal of Geophysics*, vol. 55, no. 3, pp. 998–1006, 2012.

[61] C. L. Liu, Y. G. Ye, and Q. G. Meng, "Characteristics of gas hydrate samples recovered from Shenhu area in the South China Sea," *Journal of Tropical Oceanography*, vol. 1, no. 5, pp. 1–5, 2012.

[62] X. B. Shi, Z. F. Wang, Z. P. Sun et al., "Vertical variations of geothermal parameters in rifted basinsand heat flow distribution features of the Qiongdongnan Basin," *Chinese Journal of Geophysics*, vol. 58, no. 3, pp. 939–952, 2015.

[63] L. J. Mi, Y. S. Yuan, G. C. Zhang, H. Shengbiao, H. Lijuan, and Y. Shuchun, "Characteristics and genesis of geothermal field in deep-water area of the northern South China Sea," *Acta Petrolei Sinica*, vol. 30, no. 1, pp. 27–32, 2009.

[64] X. Y. Tang, S. B. Hu, G. C. Zhang et al., "Geothermal characteristics and hydrocarbon accumulation of the northern marginal basins, South China Sea," *Chinese Journal of Geophysics*, vol. 57, no. 2, pp. 572–585, 2014.

[65] P.-B. Su, J.-Q. Liang, W. Zhang et al., "Natural gas hydrate accumulation system in the Shenhu sea area of the northern South China Sea," *Natural Gas Industry*, vol. 40, pp. 77–87, 2020.

[66] S. Kalachard and G. Harsh, "Gas hydrates in India: potential and development," *Gondwana Research*, vol. 22, pp. 645–657, 2012.

[67] D.-X. Chen, S.-G. Wu, Z.-J. Wang, and Q.-L. Sun, "Geometry and genesis of polygonal faults in epicontinental deepwater basins, northern South China Sea," *Acta Petrolei Sinica*, vol. 33, pp. 610–616, 2012.

[68] B. J. Tewksbury, J. P. Hogan, S. A. Kattenhon, C. J. Mehrtens, and E. A. Tarabees, "Polygonal faults in chalk: insights from extensive exposures of the Khoman Formation, Western Desert, Egypt," *Geology*, vol. 42, pp. 479–482, 2014.

[69] S. Ho and C. Dac, "Insights into the permeability of polygonal faults from their intersection geometries with Linear Chimneys: a case study from the Lower Congo Basin," *Carnets de géologie (Notebooks on geology)*, vol. 16, pp. 17–26, 2016.

[70] Y.-F. Li, R. H. Pu, X.-W. Fan, and B. Li, "Characteristics and genesis of the polygonal fault system in Beijiao sag of the Qiongdongnan Basin, the northern South China Sea," *Geotectonica et Metallogenia*, vol. 41, pp. 817–828, 2017.

[71] Z. Sun, Z.-X. Zhao, D. Zhou, S.-K. Yang, H.-M. Lin, and G.-H. Chen, "The stratigraphy and the sequence Achitecture of the basins in Nansha region," *Earth Science-Journal of China University of Geosciences*, vol. 36, pp. 798–806, 2011.

[72] J. Watterson, J. Walsh, A. Nicol, P. A. Nell, and P. G. Bretan, "Geometry and origin of a polygonal fault system," *Journal of the Geological Society*, vol. 157, pp. 151–162, 2000.

[73] X.-J. Wang, S.-G. Wu, D.-W. Wang, Y.-B. Ma, G.-S. Yao, and Y.-H. Gong, "The role of polygonal faults in fluid migration and gas hydrate reservoir forming in Southeast Hainan Basin," *Oil Geophys. Prospect*, vol. 45, pp. 122–128, 2010.

[74] G.-Z. Ma, H.-L. Lu, J.-A. Lu, G.-T. Hou, and Y.-H. Gong, "Polygonal fault in marine sediments and its impact on gas hydrate occurrence," *Geology in China*, vol. 47, pp. 1–13, 2020.

[75] J.-G. Zhang, *Reasearch on the Activity of Red River Fault in China and Vietnam*, University of Science and Technology of China, Anhui, 2009.

[76] S. Liu, C. Lin, X. Liu, and Q. Zhuang, "Syn-tectonic sedimentation and its linkage to fold-thrusting inthe region of Zhangjiakou, North Hebei, China," *Science China Earth Sciences*, vol. 61, pp. 681–710, 2018.

[77] X. Shi, S. Liu, and C. Lin, "Growth structures and growth strata of the Qianjiadian Basin in the western Yanshan fold and thrust belt, North China," *Science China Earth Sciences*, vol. 62, pp. 1092–1109, 2019.

[78] H. Orther, A. Kositz, E. Willingshofer, and D. Sokoutis, "Geometry of growth strata in a transpressive fold belt in field and analogue model: Gosau Group at Muttekopf, Northern Calcareous Alps, Austria," *Basin Research*, vol. 28, pp. 731–751, 2016.

[79] C. Busby, A. A. Azor, C. Busby, and A. Azor, "Modification of continental forearc basins by flat-slab subduction processes: a case study from southern Alaska," in *Tectonics of Sedimentary Basins: Recent Advances*, pp. 538–564, John Wiley & Sons, New Jersey, 2011.

[80] Y.-H. Sun, Y.-F. Lv, F. Fu, X.-F. Fu, and X.-Y. Zhang, "Evalution method on transporting natural gas efficiency of fault transportation system and its application," *Natrual Gas Geoscience*, vol. 17, pp. 73–77, 2006.

[81] G. Chen, B.-L. Bian, X. Li, G. Liu, D.-Y. Gong, and D.-L. Zeng, "Transport system and its control on reservoir formation of Jurassic-Cretacous in hinterland of Junggar Basin," *Lithologic Reservoirs*, vol. 33, no. 1, pp. 46–56, 2021.

[82] G. Fu, Z.-X. Sha, H.-W. Wang, W.-Y. Jiang, and X.-Y. Dong, "Research method and application of evolution form of oil and gas passage of oil source fault," *Chinese Journal of Geology*, vol. 57, pp. 127–138, 2022.

[83] G. Fu and S. Ge, "Evalution method and application of fault lateral sealing ability in quiescent Undiagenetic period," *Journal of Earth Sciences and Environment*, vol. 40, pp. 20–23, 2018.

[84] X.-F. Fu, D.-Q. Fang, Y.-F. Lv, G. Fu, and Y.-H. Sun, "Method of evaluating vertical sealing of faults in terms of the internal structure of fault zones," *Earth Science*, vol. 30, pp. 328–336, 2005.

[85] J. Hull, "Thickness-displacement relationships for deformation zones," *Journal of Structural Geology*, vol. 10, no. 4, pp. 431–435, 1988.

[86] H.-Q. Chen, X.-M. Zhu, G.-C. Zhang, Y.-X. Zhang, Q. Zhang, and C.-L. Liu, "Classification and combination model characteristics of pathway system in marine faulted basin: taking the Paleogene Lingshui Formation, Qiongdongnan Basin as an example," *Earth Science Frontiers*, vol. 28, pp. 282–294, 2021.

[87] D.-B. Yang, G.-Y. Zhu, J. Su, J.-J. Liu, and B. Zhang, "The passage system and effectiveness evaluation of oil and gas basin in China," *Journal of Southwest Petroleum University (Science & Technology Edition)*, vol. 33, pp. 8–17, 2011.